Research paper

Degradation and mineralization of phenol in aqueous medium by heterogeneous monopersulfate activation on nanostructured cobalt based-perovskite catalysts ACoO$_3$ (A = La, Ba, Sr and Ce): Characterization, kinetics and mechanism study

Samia Ben Hammouda [a,*], Feiping Zhao [a], Zahra Safaei [a], Varsha Srivastava [a], Deepika Lakshmi Ramasamy [a], Sidra Iftekhar [a], Simo kalliola [a], Mika Sillanpää [a,b,**]

[a] Laboratory of Green Chemistry, School of Engineering Science, Lappeenranta University of Technology, Sammonkatu 12, FI-50130 Mikkeli, Finland
[b] Department t of Civil and Environmental Engineering, Florida International University, Miami, FL 33174, USA

ARTICLE INFO

ABSTRACT

This study reports the heterogeneous catalytic degradation and mineralization of phenol in aqueous solution by means of potassium monopersulfate (PMS or Oxone) process mediated by cobalt perovskite-based catalysts (P-Co). Four nanostructured perovskites oxides with formula ACoO$_3$ (A = Ba, Ce, La, Sr) were synthesized as heterogeneous catalysts by the citrate sol gel method and characterized by means of nitrogen isotherm adsorption (BET), Scanning Electron Microscopy (SEM), Energy Dispersive X-ray Spectrometry (EDX), x-ray photoelectron spectroscopy (XPS), X-ray Diffraction (XRD), transmission electron microscopy (TEM) and Fourier transform infrared (FT-IR) techniques. All the examined samples had perovskite structure. The influences of PMS dosage, catalyst loading, initial target compound concentration and solution pH on the removal efficiency were studied. The activity showed an order of SrCoO$_3$ > LaCoO$_3$ > BaCoO$_3$ > CeCoO$_3$. LaCoO$_3$ and SrCoO$_3$ catalysts exhibit the better performance in terms of reaction rate and stability for the phenol degradation and mineralization by advanced oxidation technology based on sulfate radicals. Catalyst stability was assessed by means of consecutive reuse cycles. No significant loss of activity was noticed after five consecutive cycles. The role of reactive oxygen species produced in the system, mainly SO$_4^{\bullet-}$ and $^{\bullet}$OH, in the overall oxidation of phenol was determined by using suitable scavenger compounds. Under optimal conditions (10^{-4} M PMS, natural pH, 0.3 gL^{-1} catalyst loading) complete removal of 20 mgL^{-1} phenol was achieved in 90 min. In terms of organic carbon removal, about 81% mineralization yield was reached in the optimal conditions for 6 h heterogeneous P-Co/PMS system, suggesting an effective process for phenol mineralization. Four organics intermediates were observed and three of them were identified as catechol, hydroquinone and benzoquinone. A reaction sequence was therefore proposed for the degradation according to the detected products. Subsequent attack of these intermediates by SO$_4^{\bullet-}$ radicals led to the formation of short chain acids such as, acetic, formic and oxalic acid which were identified by ion-exclusion chromatography.

© 2017 Published by Elsevier B.V.

1. Introduction

Advanced oxidation processes (AOPs) that involve in situ-production of highly reactive oxygen species has emerged as a promising technique for the degradation of organic pollutants in water. Sulfate radicals based-advanced oxidation processes (SR-AOPs) have attracted more and more attention in the last few years, due to its greater efficiencies over a wide pH range and several operational advantages in comparison with the conventional AOPs based on hydroxyl radicals. In fact, sulfate radical (SO$_4^{\bullet-}$) possesses higher oxidation potential (2.5–3.1 V vs. NHE) as compared
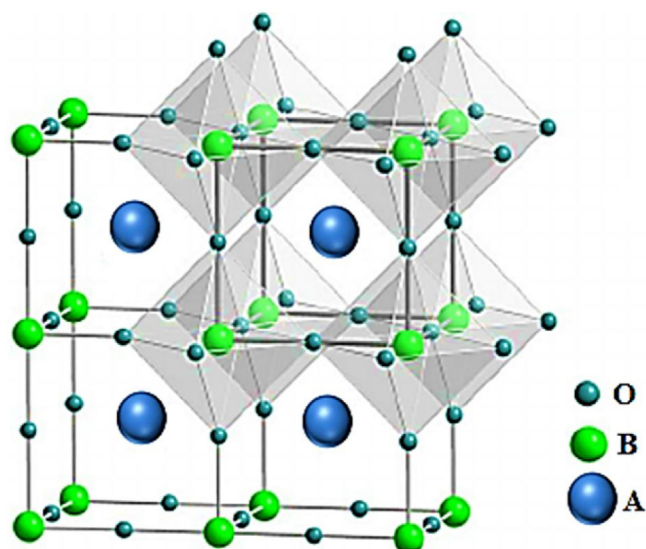
Fig. 1. Structure of a generic Perovskite crystal.

to hydroxyl radical ($\bullet$OH:1.8–2.7 V vs. NHE, pH dependent) with longer lifetime ($\sim$40 μs), which allows $SO_4^{\bullet-}$ radicals to have more stable mass transfer and greater contact with target contaminant than $\bullet$OH (life time $\sim$1 μs) [1–7].

Combination of transition metals, such as Cu^{2+}, Mn^{2+}, Fe^{2+}, and Co^{2+}, with peroxymonosulphate (PMS) as oxidant to generate sulfate radicals has been reported as a highly efficient approach and a promising alternative for water purification [8–10], with cobalt ions being the best activator [11]. Nevertheless, the use of cobalt and PMS under homogeneous system has drawbacks in terms of the cobalt leachate. Thus, to avoid the health risks associated to the adverse effect of the homogeneous Co/PMS system related to the toxicity of excessive cobalt ions, the development of cobalt-based heterogeneous catalysts has gained increasing attention.

Over the past decade, various heterogeneous cobalt-based catalysts have been applied for environmental applications through oxone activation; these were mainly unsupported cobalt oxides such as Co_3O_4 [12–14] and CoO[14], unsupported cobalt composites including iron–cobalt $CoFe_2O_4$ [15] and bismuth-cobalt oxides Co_3O_4-Bi_2O_3 [16], supported cobalt onto diverse materials such as TiO_2 [17,18], MgO [19], Silica [20,21], Al_2O_3 [21], activated carbon [22], carbon aerogel [23,24], graphene [25,26], resin [27] and zeolite [28,29]. Nevertheless, in spite of the high activity of some of these catalysts, their stability often was unsatisfactory due to leaching of the cobalt in the aqueous oxidative medium.

In the past few years, perovskites materials with a general chemical formula ABO_3, where A is a rare or alkaline earth metal and B is a first row transition metal (Fig. 1), have attracted significant research interest because of their unique physical and chemical properties that make them key components for various applications [30–39].

Recently, perovskite oxides, mainly Lanthanum based perovskite, have successfully been used for environmental application in water treatment and reported as good candidate materials for heterogeneous catalysis [40–47] due to their high activity and stability in aggressive media and at high temperature [48]. Nevertheless, to authorís knowledge, very little attention to strontium, cerium, and barium-based perovskites has been paid. The catalytic effectiveness of perovskites oxides is based on the stabilization of transition metal ions in unusual oxidation states and on the high oxygen mobility in the perovskite structure [42].

Due to its abundance in most of wastewater effluents and its toxicity, phenol is a usual organic compound model in developing methods for water remediation. Three interesting publications

were devoted to the study of catalytic properties of perovskites materials for catalytic wet hydrogen peroxide oxidation (CWPO) of phenol. Phenol was effectively oxidized in the presence of H_2O_2 by $LaTi_{1-x}Cu_xO_3$ [40], $LaFeO_3$ [41] and perovskite like oxides $LaBO_3$ (B = Fe, Cu, Mn, Ni, CO) through the hydroxyl radicals attack ($\bullet$OH) [42].

Recently, the use of perovskite structure for phenol oxidation by means of oxone activation and sulfate radical attack start to gain researchers attention. In their interesting work, C. Su et al. [49] have investigated the degradation of phenol and methylene blue by using the double perovskite oxide $PrBaCo_2O_{5+\delta}$ as an effective catalyst for PMS activation. According to the authors, the outstanding activities of the investigated catalyst for organic decontamination was attributed to superior oxygen surface exchange kinetics, abundance of active cobalt sites, and robust phase stability during the oxidation-state transition of cobalt ions. More recently, J. Miao et al. [50] have examined in their promising work the catalytic activity of various perovskites oxide $SrCo_{1-x}Ti_xO_{3-\delta}$ (x = 0.1, 0.2, 0.4, 0.6) in the activation of peroxymonosulfate for phenol under a wide pH range. They provide that perovskites based catalysts present effective degradation efficiency of aqueous contaminants with less metal leaching and higher mineralization degree.

The present work was aimed to the systematic studies of cobalt based perovskites oxides $ACoO_3$ (A = Ce, La, Ba, Sr) as efficient heterogeneous catalysts for the activation of PMS, used in the phenol degradation and mineralization in water by sulfate radicals based −advanced oxidation process. $CeCoO_3$, $SrCoO_3$ and $BaCoO_3$ oxides have never been investigated previously for water treatment application. The perovskite oxides catalysts were synthesized by the sol gel method, and characterized by means of nitrogen isotherm adsorption, scanning and transmission electron microscopy, X-ray diffraction, FT-IR and XPS. To probe in the mechanism of PMS activated by perovskite catalysts, quenching radical tests and Electron paramagnetic resonance (EPR) spectroscopic analysis was performed. The effectiveness of $ACoO_3$ and oxone combination has been investigated varying concentration, catalyst dosage and solution pH, which are the main operating variables. Catalyst reusability has also been assessed. Based on the identified cyclic intermediates and carboxylic acids as end products before mineralization, a plausible mineralization pathway was proposed.

2. Experimental

2.1. Materials

Phenol, quinone, catechol and hydroquinone were purchased from Sigma-Aldrich. Monopersulfate was acquired from Sigma-Aldrich. Barium nitrate, lanthanum nitrate, cerium nitrate, cobalt nitrate and citric acid were purchased from Sigma-Aldrich and used for perovskite synthesis. Terbutyl alcohol, methanol, acetonitrile and phosphate potassium monobasic were purchased from Sigma-Aldrich. The rest of chemicals were purchased from Sigma-Aldrich and used as received. All solutions were prepared with ultrapure water.

2.2. Catalysts preparation and characterization

Samples of $ACoO_3$ (A = Ba, Ce, La, Sr) were prepared by a citric acid sol-gel method in a way almost identical to that reported by Sotelo et al. [40]. In a typical synthesis, a solution with appropriate moles of the corresponding metal nitrate ions and excess citric acid was heated at 100 °C overnight to remove water excess. The resultant spongy pinkish material was subsequently oven-dried at 100 °C overnight. The resulting brown material was then grinded and calcinated at 700 °C for 7 h to obtain the desired perovskite

Table 1
Crystallographic parameters of the perovskites samples.

Sample	Crystal system	a (Å)	b (Å)	C (Å)	α (°)	β (°)	γ (°)	Density (g/cm³)
$BaCoO_3$	hexagonal	5.65	5.65	4.76	90	90	120	6.08
$CeCoO_3$	Cubic	5.41	5.41	5.41	90	90	90	7.21
$LaCoO_3$	Cubic	5.37	5.37	5.37	90	90	90	7.33
$SrCoO_3$	Monoclinic	4.98	5.59	9.11	90	96.28	90	5.12

structure. The resulting black $ACoO_3$ nanoparticles were washed several times with deionized water, and then dried and stored for use.

Phase compositions and particles sizes of the four synthesized materials were determined by powder x-ray diffraction (XRD) using a Co-Kα (λ = 1.7809 Å) radiation source in a PANalytical Empyrean diffractometer. The diffraction angle (2θ) ranged between 20 and 80 in 0.05° intervals. Microstructure and morphology of the synthesized materials were carried out using scanning electron microscope (SEM). The elemental composition of $ACoO_3$ (A = Ba, Ce, La and Sr) perovskite oxides was determined using Energy Dispersive X-ray Spectrometer (EDS). The EDS analysis was performed at several points and averaged to obtain the representative results.

N_2 adsorption isotherms were used for textural studies with Micromeritics' TriStar II PLUS instrument. All the studied samples were pre-degassed in vacuum at 200 °C for 2 h. Specific surface area were determined using the classical BET model. Fourier transform infrared spectra (FT-IR) were collected in the region from 400 to 4000 cm^{-1} at room temperature using a Fourier-Transform IR spectrometer. Horiba FT-730. The study of the surface composition and the electronic states of elements in the valence-band region of the perovskite oxides were recorded on a ESCALAB 250 x-ray photoelectron spectroscopy (XPS) with Al-Kα (1486,6 eV) as the X-ray source.

2.3. Experimental procedure

The treatment of phenol using oxone was conducted by batch-type experiments. Typically, the required amount of catalyst was added firstly to 100 mL of phenol solution with an initial concentration of 20 mgL^{-1} and then a known concentration of oxone was added to the solution to initiate the reaction. Samples of 1 mL were withdrawn from the reactor at set intervals and filtered immediately through a 0.22 μm filter film.

For the catalyst reusability tests, after each run the catalyst was filtrated, washed thoroughly with deionized water, and then dried at 100 °C for 1 h for reuse under similar experimental conditions.The initial pH in all experiments was not adjusted except in the experiments investigating the effect of pH.

For the identification of the reactive radicals involved in the phenol degrdation, methanol was used as effective quenching agent for both hydroxyl and sulfates radicals. Tert-butyl alcohol (TBA) was used to quench hydroxyl radicals.

2.4. Analytical methods

Phenol concentration was quantified by a Shimadzu High Performance Liquid Chromatograpy equipped with UV detection (HPLC-UV). The column used was a Kinetex C18 (5 μm, 4.6 × 150 mm). A mobile phase composed by 20 mM (phosphoric-acid) potassium buffer solution (pH 2.5) (A)and acetonitrile (B) was pumped at a flow rate of 1 mL min^{-1}, with an isocratic percentage composition of 70:30 A:B. The UV detector wavelength was set at 269 nm. Observed retention time was around 5.34 min.

Cobalt leaching was quantified by means of atomic absorption using Thermo Scientific iCAP 6000 ICP.

Generated carboxylic acids, oxalic, formic and acetic acids were identified and quantitatively followed by ion chromatography with suppressor equipped with a conductivity detector using a Shodex IC SI-50 4E (4.0 mm I.D. × 250 mm). The eluent was 3.2 mM Na_2CO_3 and 1 mM $NaHCO_3$ at a flow rate of 0.7 mL min^{-1}.

The progress of the mineralization of phenol aqueous solutions during the treatment was monitored by measuring their non-purgeable organic carbon (NPOC) abatement. The NPOC in samples was quantified by a TOC analyzer purchased from Shimadzu. Organic carbon compounds were combusted and converted to CO_2, which was detected and measured by a non-dispersive infrared detector (NDIR). Standard potassium hydrogen phthalate solutions were used as standards for the NPOC analysis.

3. Results and discussion

3.1. Characterization of $ACoO_3$ (A = La, Ba, Ce, Sr) catalysts

The as-synthesized $ACoO_3$ (A = La, Ba, Ce, Sr) samples were first characterized by powder X-ray diffraction measurements. The crystallographic parameters of the perovskites samples are illustrated in Table 1. The XRD patterns presented in Fig. 2c reveal the crystalline phase of all the samples. The results of XRD data come in agreement with those reported in literature for $BaCoO_3$ [51,52], $LaCoO_3$ [53,54], $CeCoO_3$ and $SrCoO_3$ [55]. The diffraction profiles reveal that a well-defined cubic structure was obtained for the $LaCoO_3$ and $CeCoO_3$ catalysts. $BaCoO_3$ and $SrCoO_3$ oxides are monophasic perovskites with the hexagonal and monoclinic crystal lattice, respectively, with the doublet peak at 2θ ≈ 28–29° and 30–31°. The synthesized $BaCoO_3$ sample presented weak XRD peaks, suggesting less crystallinity of this sample. It is noteworthy to mention that according to literature the crystalline structure of a perovskite catalyst is an important factor that affects its catalytic activity for different reactions [56].

According to the full width at the half-maximum of the diffraction peak, the average crystallite size of the synthesized perovskites was calculated using the Debye-Scherrer equation.

$$D(hkl) = \frac{K\lambda}{\beta Cos\theta} \tag{1}$$

Where D is the crystallite size perpendicular to the normal line of the (hkl) plane, K is the Debye-Scherrer constant (0.89), hkl the full width at half maximum (fwhm) of the (hkl) diffraction peak, hkl the Bragg angle of the (hkl) peak, and λ the X-ray wavelength.

A crystallite size in the range of 5.3 nm, 7.8 nm, 17.2 nm and 10.4 nm is observed for $LaCoO_3$, $CeCoO_3$, $BaCoO_3$ and $SrCoO_3$, respectively.

The TEM images was also employed to confirm the nanostructure size obtained from XRD. Fig. S_1 shows the typical images of (a) $LaCoO_3$, (b), (c) and (d) samples depicting spherical shaped particles with narrow size distribution; which is in accordance with the XRD results. TEM images revealed a lack of uniformity in the particle size distribution and a great homogeneity in the morphology.

Fig. 2b displays the FT- IR spectra of citric acid and the prepared $ACoO_3$ perovskites. The FTIR spectrum of the four perovskites
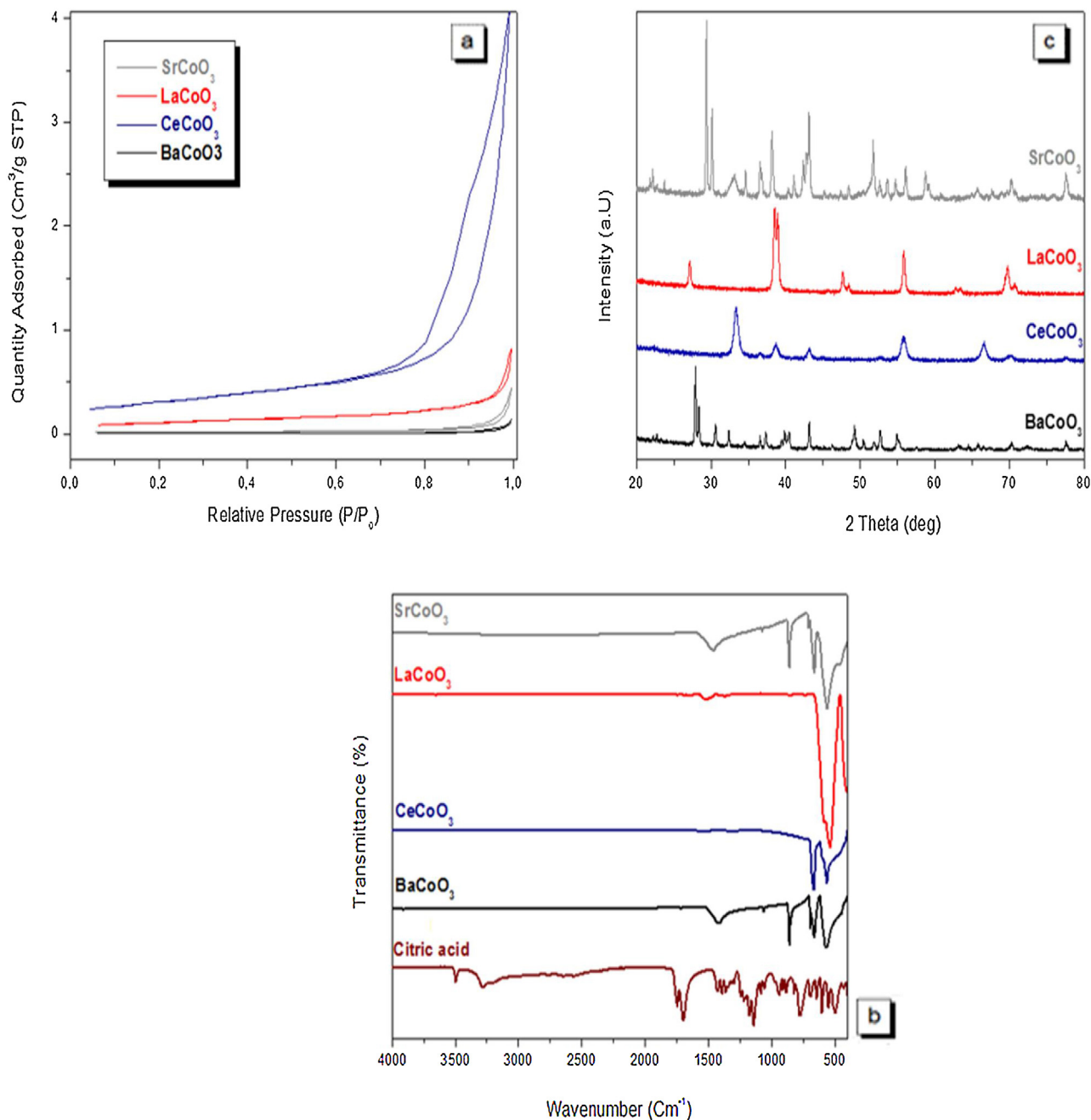
Fig. 2. (a) The nitrogen adsorption-desorption isotherms (b) The FT-IR spectra of citric acid, $BaCoO_3$, $CeCoO_3$, $LaCoO_3$ and $SrCoO_3$ perovskites, (c) XRD-Pattern of the Nano-sized $ACoO_3$ powders.

materials shows that the characteristic peaks of the organic emulsifier, i.e. citric acid, had disappeared in the calcinated products as compared with the citric acid spectra. The weak broad bands around $1500\,cm^{-1}$ $v(C=0)$ observed in $SrCoO_3$ and $BaCoO_3$ reveals the existence of residual carbonaceous, which is likely due to the incomplete combustion of organic species.

In the perovskites structure $ACoO_3$, Co and A cations could occupy the center of the octahedral BO_6 in which they have six coordinations with oxygen anions. For all perovskites sample, the most important band observed at around $530\,cm^{-1}$ could be assigned to the cobalt-oxygen stretching vibration $v(Co-0)$ of the structureís octahedrons BO_6 of the ABO_3 structure. The FTIR results are in good agreement with those obtained by XRD as mentioned above and confirm that the samples belongs to the perovskite structure.

The morphological properties of the four synthesized perovskites oxides were subsequently evaluated by SEM. It can be clearly seen from Fig. S_2 that $LaCoO_3$, $CeCoO_3$ and $SrCoO_3$ surface presents lots of nanometers size pores with high concentration of inter-particle porosity especially for $LaCoO_3$ and $CeCoO_3$, while the image of $BaCoO_3$ perovskite sample exhibits distinct grain growth into large particles. These observations are in concordance with the XRD measurements of crystallite sizes. The observed porous microstructure could be assigned to the emitted gases during the thermal decomposition of the organic species, especially water vapor (H_2O), NO_x and CO_2, among others. It can be concluded that, the gas evaporation has more effect on the porosity of $LaCoO_3$ and $CeCoO_3$ perovskites than $SrCoO_3$ and $BaCoO_3$ samples. The elemental compositions of the synthesized materials determined by
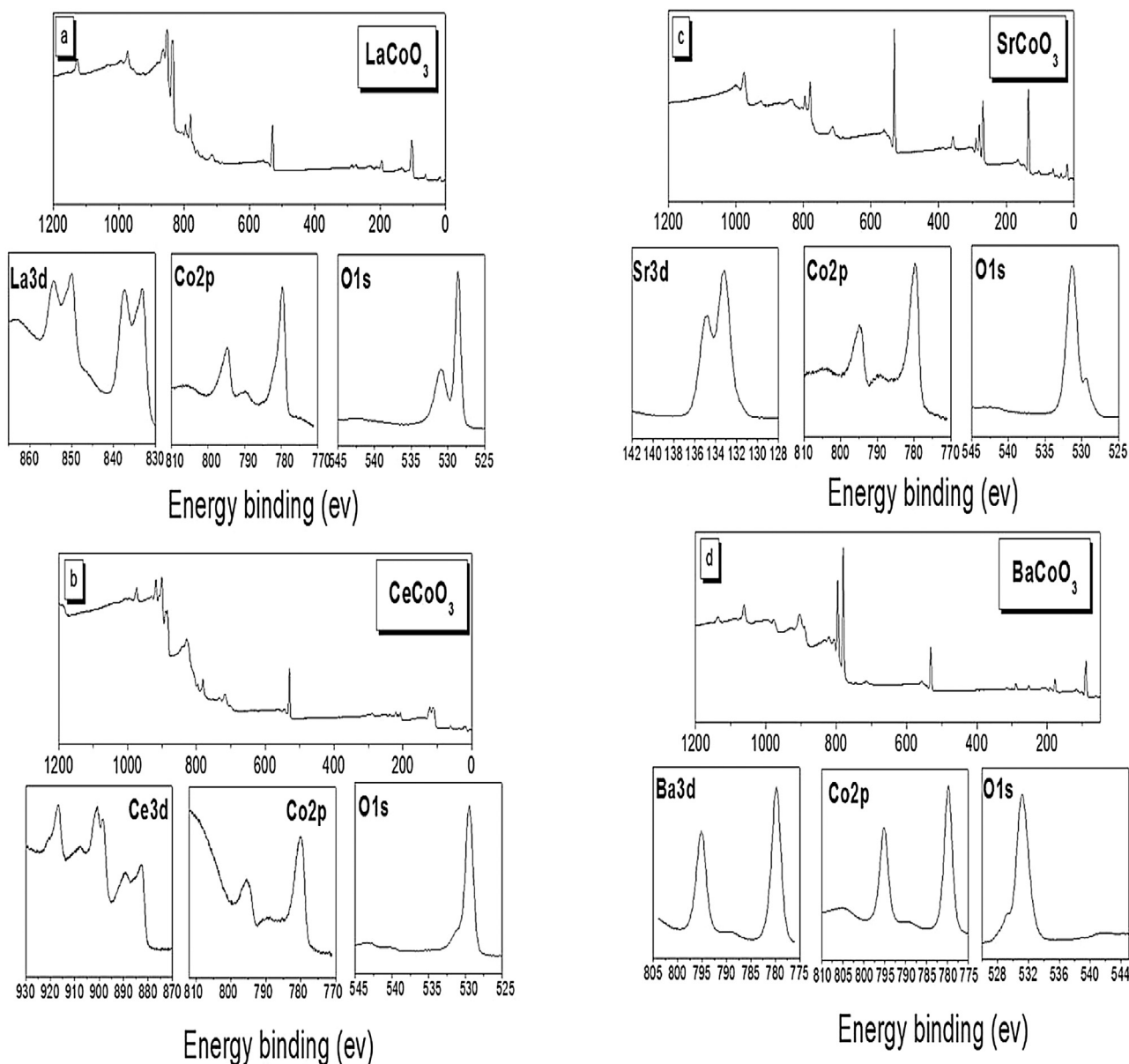
Fig. 3. The XPS spectra of (a) LaCoO$_3$ (La3d, Co2p and O1s), (b)SrCoO$_3$(La3d, Co2p and O1s), (c) CeCoO$_3$(Ce3d, Co2p and O1s) and (d) BaCoO$_3$ (Ba3d, Co2p and O1s).

Table 2
Textural properties of ACoO$_3$ (A = La, Ba, Ce, Sr) catalysts.

Sample	BET surface area (m^2 g^{-1})	Pore volume(cm^3 g^{-1})	Pore size (nm)
LaCoO$_3$	8.54	0.012	5.72
BaCoO$_3$	1.53	0.001	8.03
CeCoO$_3$	24.39	0.073	11.93
SrCoO$_3$	2.46	0.003	8.49

EDS analysis are also included in Fig. S$_1$. From this, it is possible to observe the characteristic peaks of A (A = La, Ba, Sr and Ce), Co and O in concordance to the nominal chemical composition of the envisaged perovskite materials.

The catalysts textural properties were also determined by nitrogen sorption analysis. The nitrogen adsorption-desorption isotherms of ACoO$_3$ (A = La, Ba, Ce, Sr) are exhibited in Fig. 2a. The corresponding parameters including BET surface area, pore volume and average pore size are listed in Table 2. As seen, the isotherms showed that N$_2$ adsorption was much higher on CeCoO$_3$, resulting in higher surface area and pore volume. The isotherms also indi-

cated a typical mesoporous structure of all investigated materials. LaCoO$_3$, SrCoO$_3$ and BaCoO$_3$ have the BET surface area of 8.542, 2.463, and 1.529 m^2/g, respectively; which are 3, 10 and 16 times lower than that of CeCoO$_3$.

Finally, the surface-sensitive technique, XPS, was employed to analyze the elemental proportions and the chemical state of each element in the surface of the perovskites. As shown in Fig. 3, La/Co, Ce/Co, Ba/Co, and Sr/Co could be found on the surface of LaCoO$_3$, LaCoO$_3$, LaCoO$_3$, and LaCoO$_3$, respectively. Based on the results of XPS quantitative analyses, the molar ratios of La/Co, Ce/Co, Ba/Co, and Sr/Co on the surface of the perovskites were 1.17, 1.46, 0.68, and 0.39, respectively.

In Co2p region two peaks at binding energies of 794.7 and 779.6 eV could be assigned to Co2p$_{1/2}$ and Co2p$_{3/2}$ respectively. These two peaks together with a satellite signal at 789.8 eV, which both have been reported as the characteristics of Co(III) in Co$_3$O$_4$ and LaCoO$_3$ [16,44], indicated that the cobalt on the prepared LaCoO$_3$ surface is mainly in the state of Co(III). The experimental binding energy difference between peaks Co2p$_{1/2}$ and Co2p$_{3/2}$
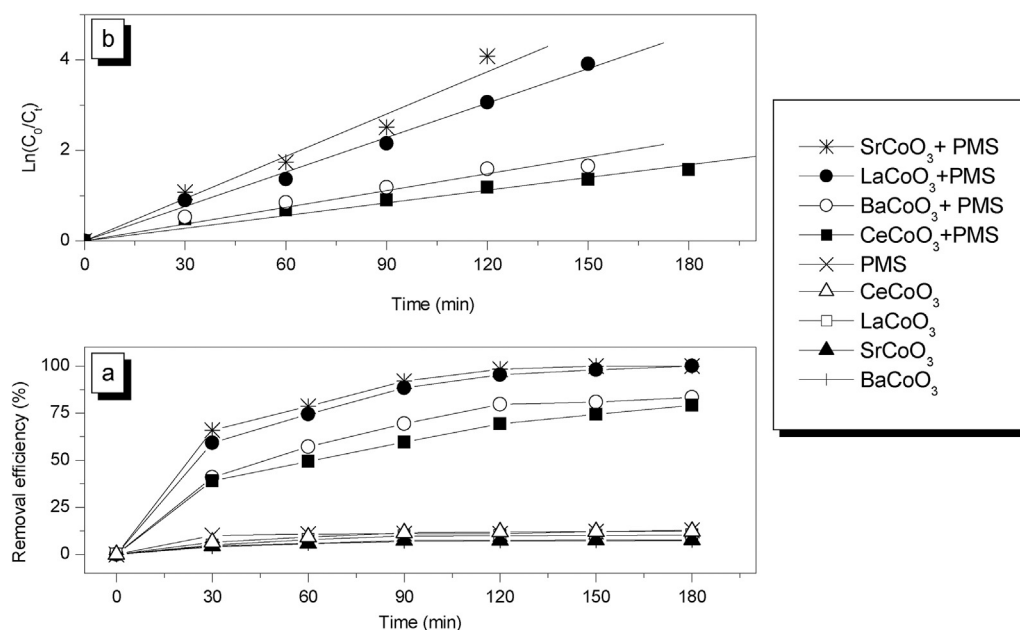
Fig. 4. (a) Adsorptive behavior of phenol (Experimental conditions: Catalyst loading 0.2 gL^{-1}, natural pH, [phenol]$_0$ = 20 mg L^{-1}, working volume = 100 mL), and its degradation behavior under PMS and P-Co/PMS system (Experimental conditions: [PMS] = 10^{-4} M, Catalyst loading 0. gL^{-1}, without pH adjustment, working volume of 100 mL, [Phenol]0 = 20 mg L^{-1}) (b) Kinetic behavior under the heterogeneous P-Co/PMS system.

(15.1 eV), which represents the second layer electronic spin-orbit splitting, was in a good consistence with the value for a reported LaCoO$_3$ (15.2 eV) [57]. Moreover, the reported characteristic peaks of Co (II) (at about 782 and 797 eV) were not observed in the perovskite, further verified this conclusion. As shown in Fig. S1c–3c, the similar peaks attributed to Co2p$_{3/2}$ and Co2p$_{1/2}$ were also observed at 780.0 and 795.5 eV in CeCoO$_3$, 779.8 and 795.1 eV in BaCoO$_3$, and 779.8 and 794.8 eV in SrCoO$_3$, respectively, suggesting the presence of Co(III) state in these perovskites.

The La3d was evaluated by a double peak for electronic spin-orbit component, which was ascribed to the strong final state of electronic configurations or energy loss phenomena (shake-up satellite). As shown in Fig. 1b, the peaks at 849.9 and 854.3 eV corresponded to La3d$_{3/2}$ and its shake-up satellite respectively, while 833.1 eV for La3d$_{5/2}$ and 837.4 eV for its satellite. These peaks coincided with the values observed in La$_2$O$_3$. In addition, the binding energy difference between peaks La3d$_{5/2}$ and La3d$_{3/2}$, which represents the third layer electronic spin-orbit splitting, equaled to 16.8 eV. This is the same as the value in the reported LaFeO$_3$, which has concluded the predominant state of La (III) in the complex oxide [42]. All these ensured the presence of La^{3+} in the perovskite. Similarly, the peaks and the peak differences in CeCoO$_3$, BaCoO$_3$, and SrCoO$_3$ (Fig. S1b–3d) were in good agreement with the corresponding literature values (e.g. Ce$_2$O$_3$ [58], BaFeO$_3$ [59], and SrFeO$_3$ [60]), ensuring that the perovskites contain trivalent cerium, barium, and strontium, respectively.

Finally, two obviously peaks were observed in O1 s region of the four prepared perovskites (Fig. 1d and Fig. S1d–S3d): the strong peaks at about 528.6 eV is the distinctive characteristic of perovskite lattice oxygen [44,57]; the other less intense peaks at about 531.0 eV could be attributed to the presence of hydroxyl groups or oxygen adsorbed on the surface of the perovskites in the atmosphere environment [44].

$$D\left(\mathbf{h}kl\right) = \frac{\mathbf{K}\lambda}{\beta \mathbf{Cos}\theta} \tag{1}$$

3.2. Phenol remediation in aqueous solutions

3.2.1. Phenol adsorption

The removal profiles of phenol versus time under different reaction conditions are shown in Fig. 4. Without the pH being controlled, control experiments were firstly performed without addition of PMS oxidant in order to examine the possibility that adsorption occurs at the perovskite catalysts interface. As seen in Fig. 4, the adsorbed amount increases slightly and reaches the plateau after about 90 min. The samples adsorb approximately between 7 and 12% of the initial pollutant concentration at 180 min, showing the weak adsorption affinities between phenol and the investigated perovskites oxides. Barium cobaltite perovskite (BaCoO$_3$), which exhibits the lowest BET surface area, shows the lowest adsorption capacity as well.

3.2.2. Oxidative decomposition of phenol

Subsequently, the degradation of phenol was carried out by the action of monopersulfate (PMS) without any catalyst addition. PMS is an unsymmetrical oxidant with redox potential of 1.82 V based on Eq. (2). It can partially oxidize some organic compounds [61].

$$HSO_5^- + 2H^+ + 2e^- \rightarrow HSO_4^- + H_2O \tag{2}$$
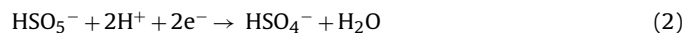
Results showed that the removal extent in this case was negligible and does not exceed 10% after 180 min of treatment, suggesting that the PMS itself could not induce significant oxidation of phenol which might be attributed to the low oxidation of PMS as compared to sulfates radicals. Similar results were observed in previous investigations. Chan et al. [14], Qi et al. [62], Deng et al. [63], Wang et al. [64] and Lin et al. [65] have reported the negligible reactivity of PMS alone towards atrazine, caffeine, diclofenac, methylene blue and Rhodamine B, respectively. Shukla et al. [66] have also investigated the phenol oxidation by another heterogeneous catalyst Co-SBA/PMS and it was reported that oxone itself in homogeneous solution could not induce significant oxidation of phenol. Ghanbari et al. [61] reported in their review that although PMS is thermodynamically a strong oxidant, its direct reaction with the majority of the pollutants is too slow so that activation is required.
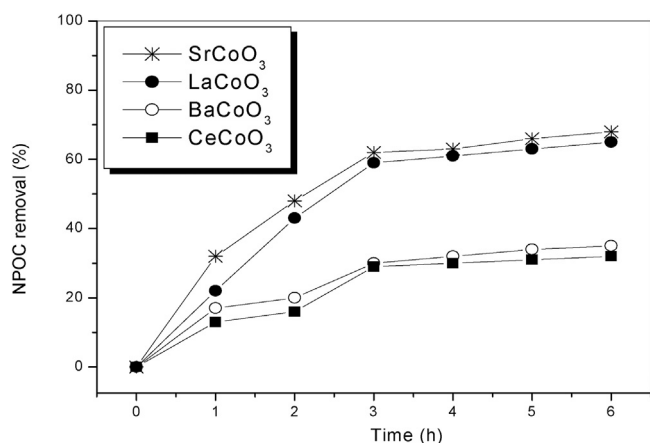
Fig. 5. Mineralization of phenol solutions (20 mg L^{-1}) by P-Co/PMS system (Experimental conditions: [PMS] = 10^{-4}, Catalyst loading 0.2 gL^{-1}, without pH adjustment, working volume of 100 mL, [Phenol]$_0$ = 20 mg L^{-1}).

3.2.3. Catalytic oxidative decomposition of phenol

Afterwards, the catalytic performance of the four prepared catalysts through phenol conversion was assessed with an initial PMS concentration of 10^{-4} M in the heterogeneous system with a catalyst dosage of 0.2 g L^{-1} and without pH adjustment. At the sight of Fig. 4a, one can see that the simultaneous presence of PMS and the cobalt based perovskites exhibit strong efficacy in the phenol oxidation and greatly enhance the removal efficiencies which increase to approximately 100%, 95%, 84% and 80% for SrCoO$_3$, LaCoO$_3$, BaCoO$_3$ and CeCoO$_3$, respectively. The significant improvement observed in the removal efficiencies of phenol was due to the activation of PMS by the cobalt based perovskites oxides which leads to the production of highly reactive oxygen entities mainly sulfate radicals. The generated sulfate radicals possess powerful oxidizing potential which can degrade phenol molecules. This result confirms the presence of lattice oxygen vacancies Co-O- in the catalysts ACoO$_3$ structure that provide reactive sites on their surface, allowing the oxidant activation.

The activities of the four investigated catalysts were in an order of SrCoO$_3$ > LaCoO$_3$ > CeCoO$_3$ > BaCoO$_3$. LaCoO$_3$ and SrCoO$_3$ showed similar activities, and they would achieve almost complete phenol removal in 120 min. Nevertheless, the reaction rate of CeCoO$_3$ and BaCoO$_3$ was slower, reaching about 80% and 75%, respectively, in the same reaction time. The difference in the catalysis efficiency of the investigated materials is probably due to the varying surface properties of the four catalysts and cobalt content.

According to previous studies relating to the heterogeneous cobalt catalysis for oxone activation, the kinetic degradation of organic compounds under this system fit a pseudo first order kinetics [20,67,68]. The kinetic behavior of the present system was evaluated and it was also determined that phenol degradation obeys the pseudo-first-order kinetic model as evidenced by the high correlation coefficients (>0.99) (Fig. 6b). The concentration profile of phenol removal can thus be represented as follows:

$$C = C_0 \exp(-k_{app}t) \tag{3}$$

Where C and C0 are the phenol concentration at time (t) and t = 0, respectively, and k is the rate constant of the first order reaction (min^{-1}). This result is consistent with the idea that the oxidative reaction of organic compounds by Co/PMS process fit second order kinetics and that the produced sulfate radicals reach a steady state after a certain operation time.

Previous investigations have been done on the phenol removal by homogeneous and heterogeneous cobalt/PMS system. Compared with the efficiency of Co^{2+} ions/PMS system in homogeneous process, the heterogeneous degradation efficiency was found to be lower. However, the catalytic potential of our synthesized perovskites oxides could be considered very high in comparison with the cobalt exchanged zeolites investigated by Shukla et al. [28] for the heterogeneous catalytic oxidation of phenol in the presence of peroxymonsulphate. Shukla et al. [28] reported complete elimination of 25 mgL^{-1} phenol in 6 h. In another work, Shukla et al. [66] observed complete removal of phenol in 180 min by using Co/SBA as catalyst for the PMS activation. Hu et al. [69] have reported a phenol removal of more than 98% after 2 h of treatment by means of peroxymonosulfate and cobalt based catalyst supported on SBA-15 mesoporous Silica. Similar phenol degradation efficiency was observed by Liang et al. [70] and 100% phenol removal could be obtained at 120 min when using mesoporous
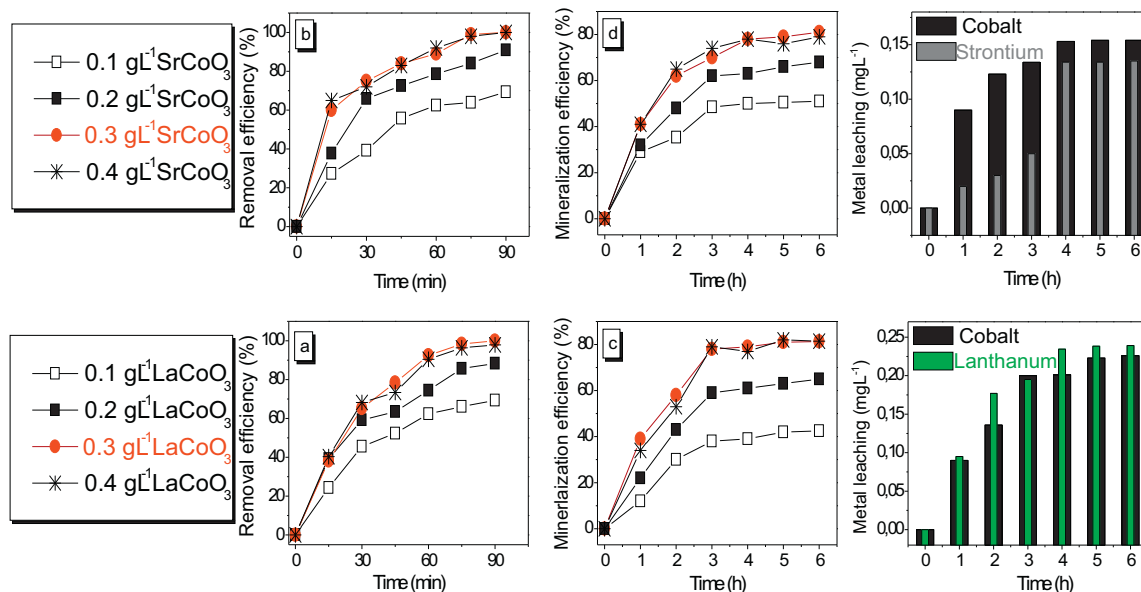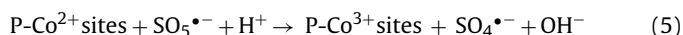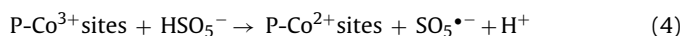

Fig. 6. Oxone mediated removal of phenol in the presence of (a,c) LaCoO$_3$ and (b,d) SrCoO$_3$. Influence of catalyst dosage. Experimental conditions: [PMS] = 1. 0 10^{-4} M, without pH adjustement^{-1}, working volume of 100 mL, [Phenol]$_0$ = 20 mg L^{-1}.

Co_3O_4/MnO_2 nanoparticles in heterogeneous activation of peroxymonosulfate.

In SR-AOPs processes, particular attention has been paid to cobalt leaching. One of the major disadvantages of cobalt heterogeneous catalysis is the catalyst deactivation due to cobalt release. Moreover, the homogeneous contribution of dissolved cobalt may distort the interpretation of the obtained results due to the high performance of homogeneous Co^{2+} metal in activating PMS. The cobalt leaching under the above conditions was checked during the 180 min of reaction using inductively coupled plasma – optical emission spectroscopy (ICP-OES) and it was found that the concentration of cobalt was below detection limit, demonstrating that the activation of PMS had occurred at the surface of the catalyst.
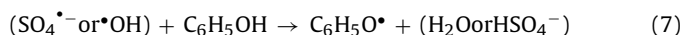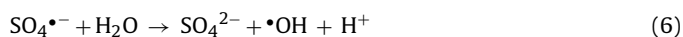
3.2.4. Possible catalytic oxidation mechanism of the heterogeneous P-Co/PMS system

The heterogeneous system for sulfate radical generation is a surface controlled process which depends mainly on PMS concentration and the catalyst properties. The phenol degradation involves firstly the surface adsorption of phenol onto the perovskite surface through electrostatic interaction and π-π stacking. Likewise, PMS is instantaneously adsorbed onto the perovskite surface and its breakage leads to the generation of powerful oxidizing species which react with phenol in solution and initiate the oxidative reaction. The possible reactions involved in the heterogeneous monopersulfate activation by cobalt-based perovskites for sulfate radical generation can be summarized by the following equations (P = Perovskite Surface):

$$P\text{-}Co^{3+}\text{sites} + HSO_5^- \rightarrow P\text{-}Co^{2+}\text{sites} + SO_5^{\bullet-} + H^+ \qquad (4)$$

$$P\text{-}Co^{2+}\text{sites} + SO_5^{\bullet-} + H^+ \rightarrow P\text{-}Co^{3+}\text{sites} + SO_4^{\bullet-} + OH^- \qquad (5)$$

Where P represents the perovskite catalystís surface.

As with the homogeneous catalysis, the mechanism of the heterogeneous system involves a one-electron transfer process: the reduction of Co(III) to Co(II) and the formation of the peroxymonosulfate radical ($SO_5^{\bullet-}$) as well as the oxidation of Co(II) to Co(III) with peroxymonosulfate and the production of sulfate radicals ($SO_4^{\bullet-}$) [12]. Subsequently, the $SO_4^{\bullet-}$ generated can react in the aqueous solution to produce hydroxyl radical and/or oxidize the phenol molecule (Eqs. (6) and (7), respectively). The oxidative attack of phenol can either take place on the perovskite surface after the adsorption of phenol molecules or in the solution after desorption of the reactive sulfate radicals from the catalyst surface.

$$SO_4^{\bullet-} + H_2O \rightarrow SO_4^{2-} + {}^\bullet OH + H^+ \qquad (6)$$

$$(SO_4^{\bullet-} \text{or} {}^\bullet OH) + C_6H_5OH \rightarrow C_6H_5O^\bullet + (H_2O \text{ or} HSO_4^-) \qquad (7)$$

By resuming, from the results of catalytic activity it can be said that all the catalysts show high activity in phenol removal. However, for practical industrial applications, the catalyst potential must be evaluated mainly in terms of its mineralization efficiency. Therefore, the investigation of mineralization degree for phenol was additionally performed under prolonged treatment (6 h) with TOC removal measurements. As shown in Fig. 5, different TOC profiles was observed. Without the catalyst, only about 5% of TOC was removed and it remained at the same level after 3 h of reaction. On the contrary, an obvious decrease up to 68% in TOC was observed when the catalyst was involved in the reaction. $SrCoO_3$ and $LaCoO_3$ nanoparticles presented much higher activity than either $BaCoO_3$ or $CeCoO_3$ in phenol mineralization. TOC measurements indicated that $CeCoO_3$, $BaCoO_3$, $LaCoO_3$ catalysts could achieve about 32%, 35, 65, 68% TOC reduction at 6 h of treatment. Moreover, Fig. 7 highlights that the TOC removal rate was faster up to 3 h and tended to decrease during the course of the P-Co/PMS treatment. The incomplete TOC removal indicates the formation of stable intermediates

which cannot be entirely mineralized in 6 h. In summary, a very considerable decrease in TOC was only observed over $LaCoO_3$ and $SrCoO_3$, the catalyst $SrCoO_3$ being more active. $LaCoO_3$ possessed smaller crystalline size and better cobalt dispersion than others catalysts due to its smaller pore size. However, Table 2 shows that BET surface area and pore volume of $CeCoO_3$ were higher than $LaCoO_3$ and $SrCoO_3$, thus the activity of $Co/LaCoO_3$ was not well related to the porous structure of the catalysts. The activities of the four catalysts were in accordance with their cobalt content, in an order of $SrCoO_3 > LaCoO_3 > BaCoO_3 > CeCoO_3$. We can conclude that higher cobalt content in the materials would lead to a more active sites for Oxone activation and a higher catalytic activity. $BaCoO_3$ and $CeCoO_3$ did not show a strong catalytic activity in terms of mineralization, these samples were not further studied in this work.

It is also worth noting that the intensity of major XRD peaks of the investigated perovskite based catalysts showed an order of $SrCoO_3 > LaCoO_3 > CeCoO_3 > BaCoO_3$. The major diffraction peak of $SrCoO_3$ was almost 3 times higher than that of $BaCoO_3$. Moreover, we observed that $CeCoO_3$ and $BaCoO_3$ had obviously lower catalytic activity than $SrCoO_3$ and $LaCoO_3$. Therefore, lower crystallinity should be one of the main reasons for the lower catalytic activity observed with barium and cerium perovskite based catalysts. We also suggest that the crystal structure properties can be studied with regard to the impact of the atomic radius on the structural parameters. Barium possesses the higher atomic radius 270 nm and the lower catalytic activity was obtained with its corresponding perovskites oxide $BaCoO_3$. The best catalytic performance has been observed with the perovskite catalyst obtained from strontium which possesses the lower atomic radius and; thus, the lower distance between both cobalt and oxygen atoms. The authors conclude that perovskites with smaller atomic radius correlated to the better coordination between atom A and B or oxygen, leading to higher crystallinity and better catalytic activity.

3.2.5. Influence of catalyst concentration

Since $LaCoO_3$ and $SrCoO_3$ catalysts showed an outstanding performance on phenol degradation and mineralization through the PMS activation, further PMS activation studies were performed by using different catalyst dosages (0.1, 0.2, 0.3 and 0.4 g L^{-1}) at 25 °C under a monopersulfate concentration of 10^{-4} mol L^{-1}. The profiles of phenol degradation with the reaction time for various $SrCoO_3$ and $LaCoO_3$ catalysts dosage are displayed in Fig. 6a and b. It can clearly be seen that the increase in the amount catalyst was accompanied by an enhancement in the removal efficiency. The higher the cobalt based catalyst loading, the faster was the degradation rate. This improvement of catalytic activity with the increasing of catalyst loading is confirmed from the profiles of TOC removal shown in Fig. 6c and d. For $SrCoO_3$ and $LaCoO_3$, respectively, after 90 min of treatment, phenol degradation reaches approximately 70, and 68% at 0.1 g L^{-1}, while the efficiency increases to 100% when increasing catalyst loading to 0.3 g L^{-1}. These results clearly indicate that the increased availability of active cobalt sites in the solution induce a better interaction with monopersulfate for the promotion of more free sulfate radicals which denotes the role played by the perovskite oxides catalysts in the radicals production. However, no further increase in the removal efficiency of phenol was observed for catalyst loading beyond 0.3 g L^{-1}, which can be ascribed to some parasitic surface reactions. As a rule of thumb, excessive metallic co sites can act as a sulfate radical scavenger to form other non-oxidizing entities, reducing the radicals available for phenol decay.

Interestingly, results show that the extent of cobalt leached was negligible for all the tested catalyst loading, and regardless of the investigated catalyst which indicates a high stability of the synthesized catalysts. In addition, it is noteworthy that the cobalt leaching concentration increased with increased P-Co dosage, with
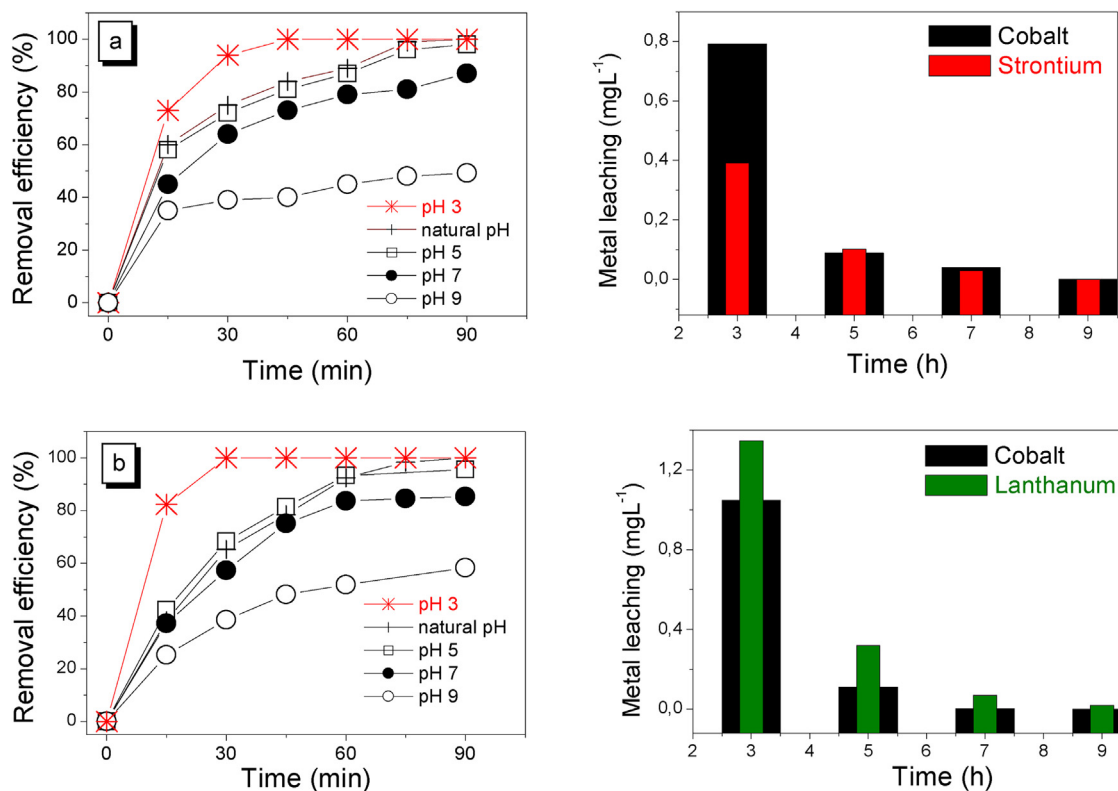
Fig. 7. Oxone mediated removal of phenol in the presence of (a) SrCoO$_3$ and (b) LaCoO$_3$. Influence of initial pH solution. Experimental conditions: [PMS] = 1. 0 10^{-4} M, Catalyst loading 0.3 gL^{-1}, working volume of 100 mL, [Phenol]$_0$ = 20 mg L^{-1}.

Table 3
Phenol removal percentage and cobalt leached after 30 min at various PMS concentration (experimental conditions as in Fig. 9.

Catalyst	Oxidant concentration (M)	Phenol removal (%)	TOC (%)	Cobalt leaching(mgL^{-1})
	10^{-5}	37.76	15.65	<0.0001
LaCoO$_3$	10^{-4}	65.22	27.34	0.119
	0.5 10^{-3}	100	37.09	0.803
	10^{-5}	39.89	17.02	< 0.0001
SrCoO$_3$	10^{-4}	75.32	29.66	0.103
	0.5 10^{-3}	95.67	38.78	1.167

0.156 mgL^{-1} and 0.132 mgL^{-1} at the highest dosage of 0.4 gL^{-1} for LaCoO$_3$ and SrCoO$_3$, respectively.

In order to evaluate the impact of catalyst loading on the mineralization efficiency, the TOC values degree reached in the reaction during 6 h of treatment were followed. The mineralization degree after 6 h of reaction was comprised between 51.4 and 81.9% for SrCoO$_3$ and between 42.5 and 81.3% for LaCoO$_3$. In order to study the possible contribution of homogeneous cobalt to the phenol mineralization, the leaching of the metals has been followed during mineralization. Fig. 6 shows the amount of active metal species leached off into the aqueous solution after 6 h of reaction in the presence of 0.3 g L^{-1} catalyst concentration, which was considered as optimal catalyst loading. It can be seen that, regardless the elapsed reaction time, under our experimental conditions the amount of cobalt in solution are negligible, below 0.25 mgL^{-1}, which discards the contribution of the homogeneous Cobalt/PMS reaction and indicates the high stability of cobalt, lanthanum and strontium species in the perovskite oxide network.

3.2.6. Influence of oxidant dosage

It is well known that, the catalyst efficiency is affected not only by the concentration of active metal sites but also by the oxidant concentration that means by the PMS to active centers ratio. Sulfate radicals based advanced oxidation processes are accompanied by the production of sulfate ions as a principal byproduct from the catalytic oxidation reaction between the organic contaminants and active radicals. Referred to the U.S. environmental protection agency, the maximum contaminant level for sulfate in drinking water is 250 mgL^{-1} which corresponds to around 400 mgL^{-1} (0.65 mM) of oxone dosage [71,72].

Besides the risk of secondary contamination by sulfate anions, it is worthwhile to take into account that, in order to make the SR-AOPs competitive with other AOPs, it is crucial to keep operating costs as low as possible, which necessarily imply to have low consumption of the oxidizing agent Oxone. In this regards, herein the study of the PMS effect on phenol conversion was limited in the range [10^{-5}–0.5 10^{-3}M].

PMS concentrations of 10^{-5}, 10^{-4} and 0.510^{-3} M were assessed for SR-AOP at 25 °C, without controlling the solution pH in the presence of 0.3 g L^{-1} of ACoO$_3$ (A = Sr or La) (Table 3). Data are reported as phenol and TOC removal along the reaction.

It was reported that the further increase in PMS dosage would result in lower degradation efficiency and rate for the organic pollutants in the system of cobalt-based catalyst and PMS due to self-quenching of sulfate radicals by PMS [8,70]. However, the neg-
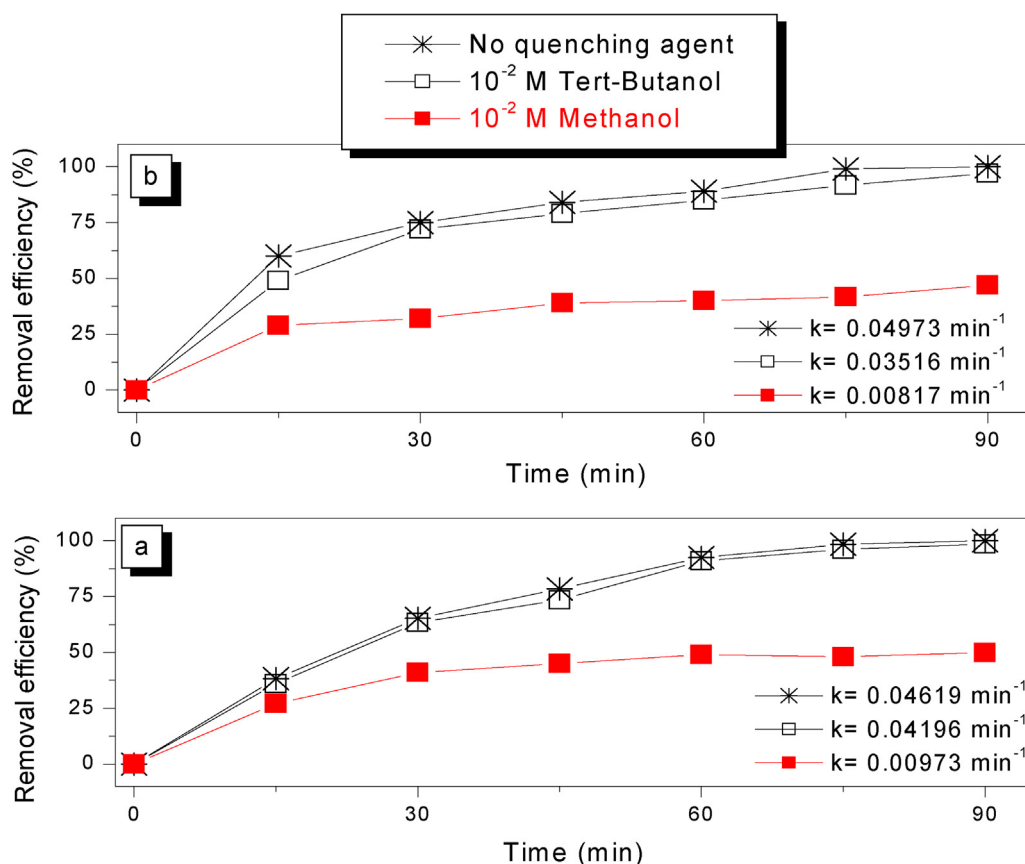
Fig. 8. PMS mediated removal of phenol in presence of (a) LaCoO$_3$ and (b) SrCoO$_3$. Influence of scavengers presence. Experimental conditions: [PMS] = 1. 0 10^{-4} M, Catalyst loading 0.3 gL^{-1}, without pH adjustment, working volume of 100 mL, [Phenol]$_0$ = 20 mg L^{-1}.

ative impact of the higher PMS dosages on phenol degradation efficiency was not observed in this work. The phenol transformation via PMS activation using both cobalt catalysts at various PMS concentration after 30 min of treatment are illustrated in Table 3. From this table, it is evidenced that the increase in the oxidant concentration enhances significantly the TOC and phenol removal. Extremely high activation with complete and approximately 96% conversion of phenol within 30 min was observed in the presence of 0.5 10^{-3} M PMS concentration and 0.3 gL^{-1} of SrCoO$_3$ and LaCoO$_3$, respectively. A negligible amount of cobalt was detected in the aqueous solution after reaction with 10^{-4} M PMS. However, it must be noted that at higher oxidant concentration a significant leaching of cobalt was observed. The high enhancement and the rapid phenol conversion observed at 0.5 10^{-3} M is ascribed mainly to the leaching of cobalt and the contribution of the homogeneous concentration on the PMS activation. By increasing oxidant concentration a significant increase of leaching is observed. The Co leaching concentration ranged from 0 to 0.803 and from 0 to 1.167 mg L^{-1} for SrCoO$_3$ and LaCoO$_3$ respectively. This result can be ascribed to the fact that PMS is an acidic oxidant; thus, PMS addition led to decrease in the solution pH, which was substantial in the cases that high PMS doses were used. It was experimentally found that the initial phenol solution pH decreases from 5.6 to 4.7 when 10^{-4} M of PMS was used and to 3.1 when the PMS concentration was 0.5 10^{-3} M. To avoid this problem of pH decrease observed at relative PMS high concentration, alkali or buffers must be added to keep neutral conditions for the reactions, which will increase the treatment costs and contribute to a new pollution. Hence, for all the reasons mentioned above, oxone concentration of 10^{-4} was chosen as optimal oxidant concentration for next experiments.

3.2.7. pH effect on catalytic performance and potential metal ion leaching

As mentioned in the paragraph above, the pH seems to have a great influence on the stability and catalytic activity of the heterogeneous perovskite catalysts. To further confirm the negative impact of acidic pH on the catalyst stability, leached cobalt and phenol degradation at different initial pHs were investigated in the following experiments. The pH effect was examined at 3, 5, 7 and 9, corresponding to acidic, neutral and basic conditions, respectively. Concentration of [H$^+$] in the reaction was maintained by using buffer solutions. The degradation at the unadjusted initial pH (i.e., 5,3) is also included in Fig. 7 for comparison. As is shown, acidic condition was favorable for the phenol degradation, the fastest and highest overall removal was observed at pH 3. The phenol removal efficiency gradually decreases with the increase of pH. Increase of the initial pH from 3 to 9 causes a significant drop in removal efficiency to about 50% and 47% for LaCoO$_3$ and SrCoO$_3$, respectively. In fact, at basic conditions, hydroxyl radicals would scavenge sulfate radicals and become the dominator species, which possesses weaker oxidation potential and shorter lifetime than SO$_4^{\bullet-}$ Eq. (8). Another possible reason for the inhibited removal at high pH is the self-dissociation of oxone. Above pH 7, the active oxygen of PMS starts to decompose; therefore less sulfate radicals are available for phenol degradation [73,74].

$$SO_4^{\bullet-} + OH^- \rightarrow {}^{\bullet}OH + SO_4^{2-} \tag{8}$$

As expected, the results show that highly acidic medium affects negatively the stability of cobalt-based perovskites catalysts. A significant leaching of cobalt to water bulk was observed at pH 3. The leached cobalt concentration from LaCoO$_3$ was 1.047, 0.117, 0.0025 and <0.0001 at pH, 3, 5, 7 and 9 respectively. For SrCoO$_3$,
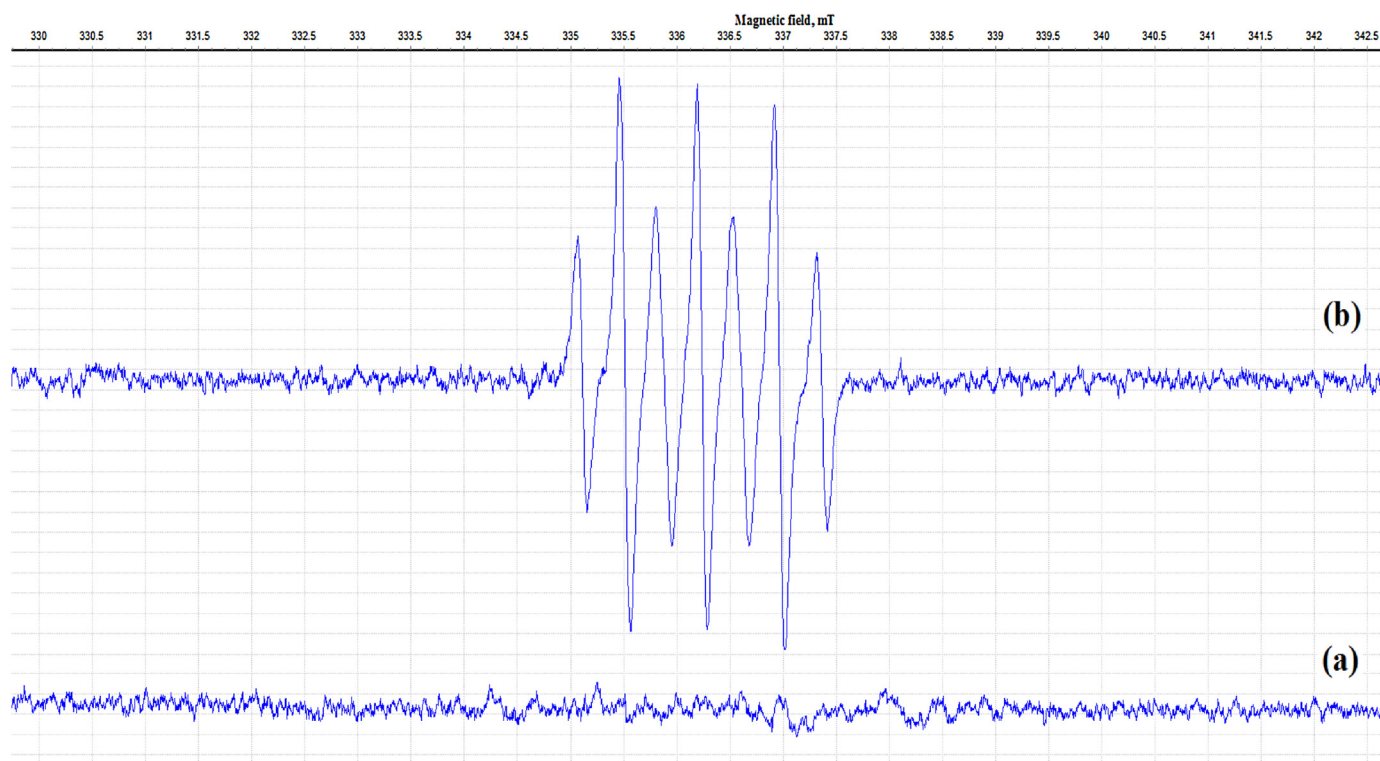
Fig. 9. ESR spectra of (a) PMS alone and (b) P-Co/PMS (b) in water.

the extent of leached cobalt was lower compared to $LaCoO_3$ and an amount of 0.792, 0.089 and 0.04 mgL^{-1} was observed at pH 3, 5 and 7 respectively. Under the significant release of cobalt at pH 3, the homogeneous Co/PMS reaction would contribute with the heterogeneous path to the phenol elimination.

In order to evaluate the contribution of the homogenous reaction during the overall heterogeneous PMS/Catalyst reaction at pH 3, a further experiment was conducted using only the aqueous cobalt ions produced by $LaCoO_3$ and $SrCoO_3$ dissolution as the catalyst. The homogeneous reaction was carried out by removing ABO_3 catalyst after vigorous agitation for 2 h and then adding 10^{-4} PMS in the filtrate. Results showed that the homogenous Cobalt/PMS reaction resulted in 48% and 37% phenol removal for $LaCoO_3$ and $SrCoO_3$, respectively (the detailed results are not shown). This finding confirms that, at pH 3, the surface catalyzed process and the dissolved cobalt ions contribute together in the phenol degradation through the generation of sulfate radicals.

The homogeneous contribution was also examined at unadjusted pH by conducting experiments in the presence of 0.125 and 0.103 mgL^{-1} of cobalt, which is the observed cobalt lixiviated from $LaCoO_3$ and $SrCoO_3$, respectively, at natural pH after 90 min of reaction. The removal efficiencies were similar to those obtained in the presence of PMS and without addition of catalyst. Thus, it can be concluded that the phenol oxidation by means of the ABO_3/PMS system at pH above 5 and in the presence of relatively low concentration of PMS (10^{-4} M) occurs as a result of the reaction between PMS and cobalt sites present on the perovskites surface, which generates sulfate radicals in adequate conditions for attacking adsorbed phenol molecules. However, leached iron from ABO_3 observed at pH 3 could contribute significantly to phenol removal.
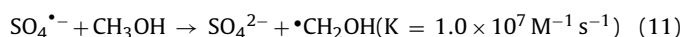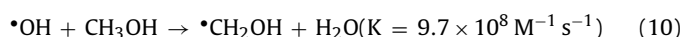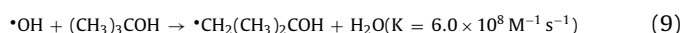
The observed negative effect of acidic medium is in accordance with many evidences which have shown that heterogeneous cobalt catalysts, such as Co_3O_4 and $Co(OH)_2$ [75] [76], are not stable under acidic conditions. A relatively high cobalt release at low pH conditions causes secondary pollution and impedes the reuse of the

heterogeneous catalyst [77]. Therefore, after analyzing the trade-off between catalytic performances, leaching levels and operational cost, natural pH was chosen as the optimal. Thus, pH was not adjusted for all subsequent runs.

3.2.8. Identification of reactive species

Sulfate radical-based oxidation system is characterized by the coexistence possibility of sulfate ($SO_4^{\bullet-}$) and Hydroxyl ($\bullet OH$) Radicals. In a view of the difference in their attack pathway on the target pollutant, it is important to determine the main reactive radical involved in the SR-AOP system.

Thus, quenching runs were conducted to determine the principal reactive oxygen species generated from oxone activation by the investigated cobalt based perovskites catalysts; the results are displayed in Fig. 8. Tert-butyl alcohol (TBA), a typical hydroxyl radical scavenger frequently used to discriminate between the participations of $\bullet OH$ and $SO_4^{\bullet-}$ in the overall pollutant oxidation in SR-AOP systems, was firstly evaluated. It was observed that 10^{-3} M TBA has almost no inhibitory effect on the phenol degradation. Further increase in the ter-butyl alcohol to 10^{-2} M does not improve the inhibition, suggesting that $\bullet OH$ was not strongly involved during the oxidation of phenol and the major entities generated in the given reaction are sulfate radicals. It should be noted that TBA reactivity with $SO_4^{\bullet-}$ ($K = 4.0 \times 10^5\,M^{-1}\,s^{-1}$) [78] is considerably poor as compared to that of $\bullet OH$ ($K = 6.0 \times 10^8\,M^{-1}\,s^{-1}$) [79] which can be explained by the high TBA susceptibility to the hydrogen abstraction by $\bullet OH$, while $SO_4^{\bullet-}$ reacts preferentially via the electron transfer reaction.

$$\bullet OH + (CH_3)_3COH \rightarrow \bullet CH_2(CH_3)_2COH + H_2O(K = 6.0 \times 10^8\,M^{-1}\,s^{-1}) \quad (9)$$

$$\bullet OH + CH_3OH \rightarrow \bullet CH_2OH + H_2O(K = 9.7 \times 10^8\,M^{-1}\,s^{-1}) \quad (10)$$

$$SO_4^{\bullet-} + CH_3OH \rightarrow SO_4^{2-} + \bullet CH_2OH(K = 1.0 \times 10^7\,M^{-1}\,s^{-1}) \quad (11)$$

The effect of Methanol, which is commonly used as a chemical scavenger to suppress the contributiion of both hydroxyl and

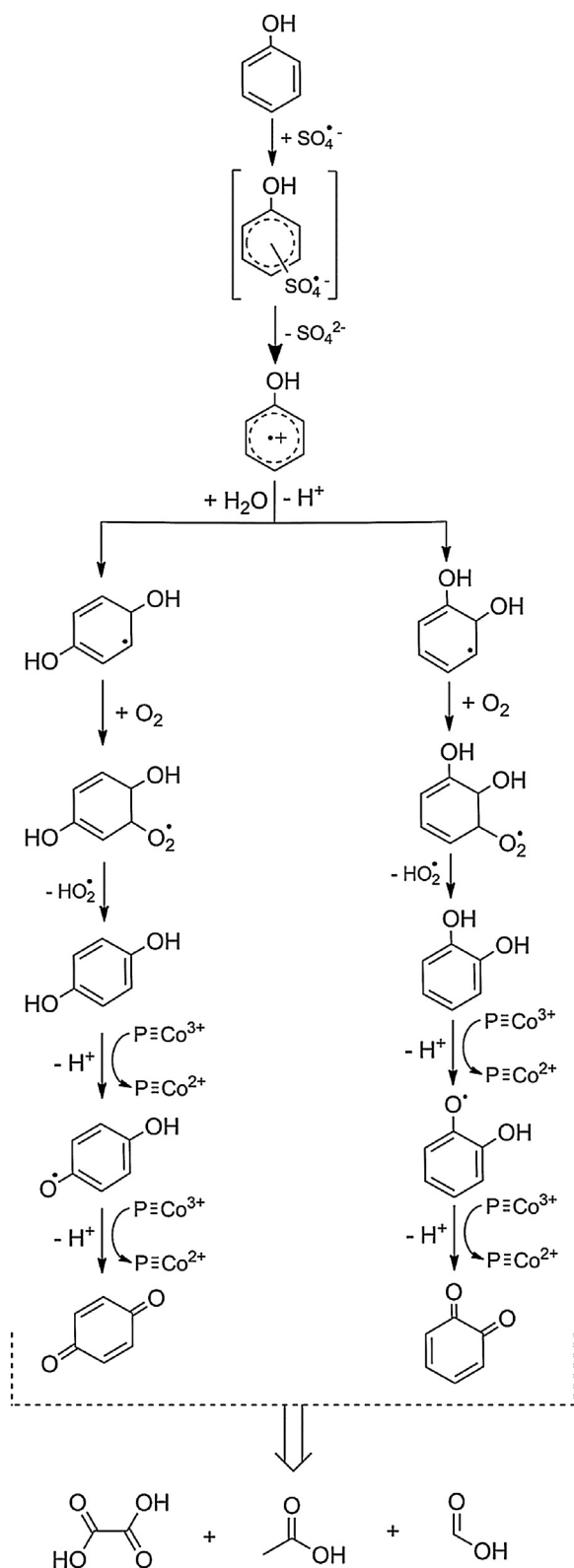**Fig. 10.** Possible pathway of Phenol oxidation with nanostructured perovskites structures.

Fig. 11. Evolution of short-chain organic acids in the oxidation of 100 mgL^{-1} phenol under P-Co/Oxone system.

sulfate radicals (Eqs. (10) and (11)), was also assessed to quantify by indirect kinetic approach the relative contributions of •OH and SO$_4^{•-}$ in the investigated SR-AOP system. In the presence of MeOH, the degradation efficiency was substantially hindered and decreased to about 50% for both catalysts in the reaction time
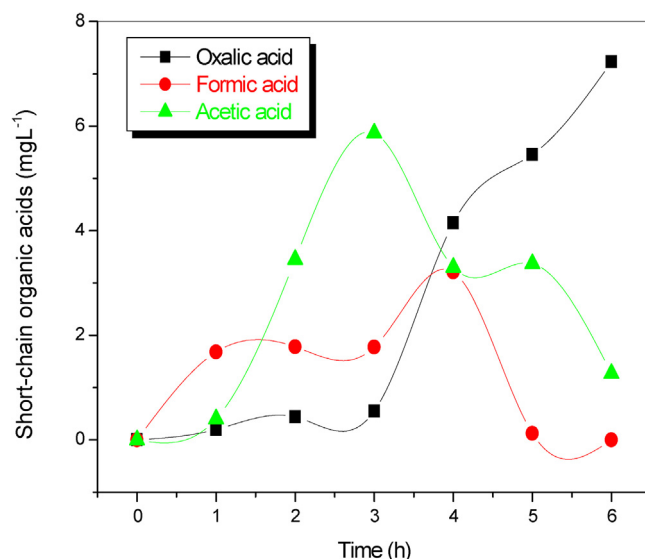
of 90 min, indicating that sulfate radicals were the major radical species involved during the oxidation. The relative contribution of sulfate radicals (>97%) was calculated by comparing the difference in the removal efficiencies of the phenol removal with and without hydroxyl radical's scavenger addition.

$$\text{\% Sulfate radicals contribution} = \frac{\text{\% removal with • OH scavenger}}{\text{\% removal without • OH scavenger}} \quad (12)$$

To further confirm that the radical entities produced during the activation of oxone by the cobalt based perovskite catalysts are sulfate radicals, EPR spectroscopy was also employed. Fig. 9 displays EPR spectra of PMS with and without catalyst using DMPO as the free radical spin trapping agent. No noticeable signal was observed when PMS alone was dissociated in water, indicating no formation of DMPO-adducts. Interestingly, as can be seen in Fig. 9, by the addition of the cobalt based catalyst to the PMS solution, a seven-line pattern was detected, which is in good accordance with the pattern reported by Lin et al. [80] and Qian et al. [81] for sulfate radicals in absence of hydroxyl radicals.

3.2.9. Phenol degradation pathway

HPLC analysis indicated that the gradual disappearance of phenol peak was accompanied by the appearance of four main new peaks which appears at retention times of 2.6, 3.1, 3.8 and 4.0 min.

Based on the phenol intermediates reported in literature, herein, the byproducts identification was made by comparison between samples and standards compounds. The major possible intermediate products detected were identified as catechol, hydroquinone and benzoquinone. The products with retention time 3.1 could not be identified. From these results, the mechanism of phenol oxidation following a sulfate radical attack through the PMS/ACoO$_3$ system is summarized in Fig. 11.

Initially, sulfate radicals attack phenol to form the unstable hydroxycyclohexadienyl radical as illustrated in Fig. 10. The hydrolysis of this latter induce the generation of hydroxylated radical entities which will undergo reaction with the O$_2$ produced from the decomposition of oxone leading to the formation of the stable by-products Catechol (benzene-1,2-diol)and hydroquinone (benzene-1,4-diol) upon hydroxylation of the aromatic ring. The hydroquinone formation is followed by subsequent hydrogen atom
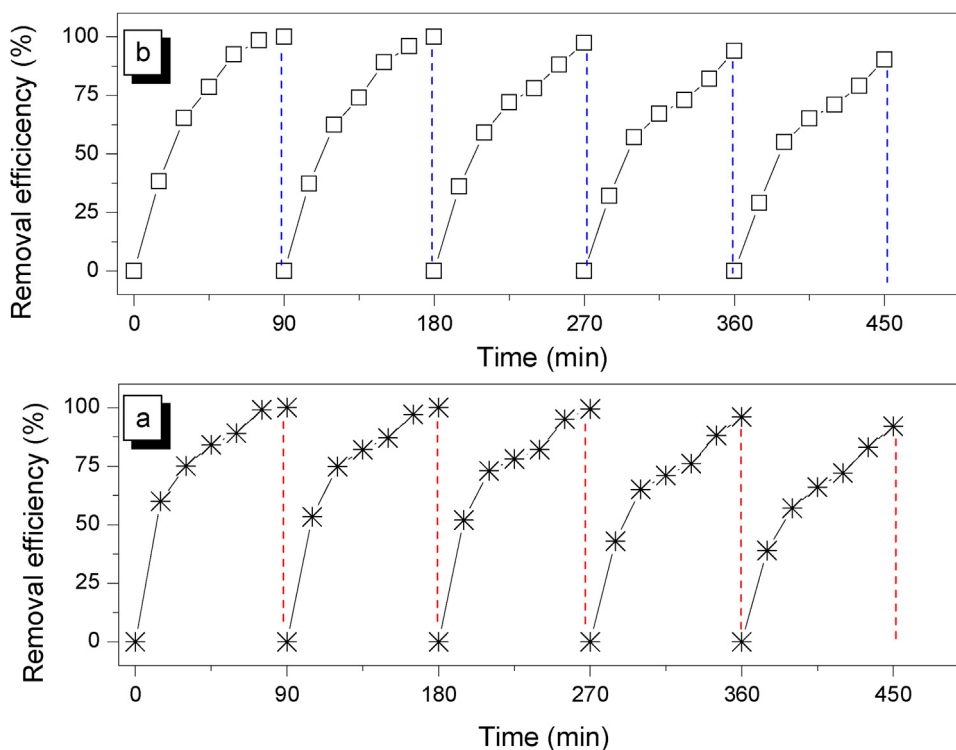
Fig. 12. Degradation profile of phenol under the heterogeneous P-Co/PMS process with recycling of the (a) $SrCoO_3$ and (b) $LaCoO_3$ catalysts. Experimental conditions: [PMS] = 10^{-4} M, Catalyst loading 0.3 gL^{-1}, without pH adjustment, working volume of 100 mL, [Phenol]$_0$ = 20 mgL^{-1}).

abstraction reaction, either by the reduction of cobalt (III) or via the decomposition of oxone which give rise to the formation of p-benzoquinone intermediate. Likewise, hydrogen atom abstraction reaction on catechol can lead to the o.benzoquinone formation. Finally, the ring is opened to form aliphatic acids that are then mineralized. It is noteworthy that, the three major byproducts identified here, from the sulfate radical based oxidation of phenol, have been also reported in hydroxyl radical processes studies such as the Fenton process [82], sonolysis [83], ozonolysis [84] and photocatalysis [85] and as well in an interesting work of Anipsitakis et al. dedicated to the homogeneous cobalt-mediated activation of peroxymonosulfate and sulfate radical attack of phenol [8]. We do not exclude the possibilities of other unidentified products formation in the reaction process. With further oxidation, the $SO^{\bullet-}$ would lead to benzene ring opening and the formation of low-molecular-weight organic acids.

The final analysis of samples after 5 h of P-Co/PMS treatment indicated the complete removal of all these organic compounds, which confirms that their further oxidation led to the formation of short chain carboxylic acids which are the last secondary degradation products before mineralization, Oxalic acid (tr = 23.45 min), acetic acid (tr = 5.75 min), and formic acid (tr = 6.24 min) were the main acids identified by ion chromatography in the final stage of phenol degradation; their retention times were compared with standard compounds. It should be noted that the corresponding experiment was conducted at high concentration (100 mgL^{-1}) in order to ensure their detection. As can be seen from Fig. 11, even after 480 min oxalic and acetic acids were not totally removed. The high persistence of these compounds explains the incomplete mineralization of phenol reported in the above discussions. A similar trend was observed by Zazo et al. [86] during the catalytic wet peroxide oxide of phenol with a Fe/active carbon catalyst.

3.2.10. Stability of nano-CeCoO₃ and LaCoO₃ catalysts after multiple runs: catalyst recyclability

It is well-known that the economic viability of the heterogeneous catalytic advanced oxidation processes is linked to the catalyst reuse possibilities. Thus, as heterogeneous catalysts, the recyclability of the lanthanum and strontium cobalt based perovskites oxides for activating PMS for phenol degradation is an important aspect. Therefore, five consecutive recycling runs of the nano catalysts were conducted. The used $ACoO_3$ (A = Sr, La) was collected dried and added to the subsequent experiment without any regeneration treatment. As observed in Fig. 12, the reused catalysts exhibit good performance and stability over 5 cycles. The removal efficiency of phenol by $SrCoO_3$/PMS system remained almost the same compared to the fresh catalyst for three cycles. In the fourth and fifth cycle, phenol degradation efficiency showed a very slight decrease to about 96% and 92% respectively. Likewise, $LaCoO_3$ presents a strong stability and activity which remained unaffected until the third run and decreased slightly in the fourth run. The slight decrease observed after several reuse may be caused by active sites blockage. In summary, one can conclude that $SrCoO_3$ and $LaCoO_3$ are recyclable, stable and promising heterogeneous catalysts for PMS activation.

4. Conclusions

$SrCoO_3$ and $LaCoO_3$ exhibited a high activity in PMS activation for phenol degradation and mineralization in aqueous solution by means of sulfate radicals attack. Phenol degradation followed the pseudo first order kinetics. Phenol oxidation gives rise to three aromatic intermediates which finally disappear completely evolving to short-chain organic acids. Oxalic acid showed to be fairly refractory to oxidation being responsible for the residual organic carbon. Thus, a possible degradation pathway was proposed. Perovskite based catalyst was found to be able to activate oxone for phenol oxida-

tion over multiple cycles without changing its catalytic activity. It was found that the heterogeneous character of the nano perovskite oxides was more pronounced at pH above 5, as indicated by the good degradation efficiency and low cobalt leaching, resulting in a long-term stability. In summary, cobalt-based perovskite catalysts can be considered as a promising heterogeneous catalyst for organic oxidation by means of sulfate radicals attack.

Appendix A. Supplementary data

Supplementary data associated with this article can be found, in the online version, at http://dx.doi.org/10.1016/j.apcatb.2017.05.051.

References

[1] G.P. Anipsitakis, D.D. Dionysiou, Environ. Sci. Technol. 37 (2003) 4790–4797.
[2] P. Hu, M. Long, Appl. Catal. B: Environ. 181 (2016) 103–117.
[3] H. Liu, N. Zhang, Z. Zhu, Chin. Sci. Bull. (Chin. Version) 57 (2012) 3493–3499.
[4] M.G. Antoniou, A.A. de la Cruz, D.D. Dionysiou, Appl. Catal. B: Environ. 96 (2010) 290–298.
[5] R. Yuan, S.N. Ramjaun, Z. Wang, J. Liu, J. Hazard. Mater. 196 (2011) 173–179.
[6] S. Yang, Y. Chen, H. Hu, P. Wang, Y. Liu, M. Wang, Prog. Chem. 20 (2008) 1433–1438.
[7] Y.-F. Huang, Y.-H. Huang, J. Hazard. Mater. 162 (2009) 1211–1216.
[8] L. Hu, F. Yang, W. Lu, Y. Hao, H. Yuan, Appl. Catal. B: Environ. 134–135 (2013) 7–18.
[9] G.P. Anipsitakis, D.D. Dionysiou, Appl. Catal. B: Environ. 54 (2004) 155–163.
[10] G.P. Anipsitakis, D.D. Dionysiou, M.A. Gonzalez, Environ. Sci. Technol. 40 (2006) 1000–1007.
[11] G.P. Anipsitakis, D.D. Dionysiou, Environ. Sci. Technol. 38 (2004) 3705–3712.
[12] X.Y. Chen, J.W. Chen, X.L. Qiao, D.G. Wang, X.Y. Cai, Appl. Catal. B: Environ. 80 (2008) 112–116.
[13] G.P. Anipsitakis, E. Stathatos, D.D. Dionysiou, J. Phys. Chem. B 109 (2005) 13052–13055.
[14] K.H. Chan, W. Chu, Water Res. 43 (2009) 2513–2521.
[15] Q. Yang, H. Choi, S.R. Al-Abed, D.D. Dionysiou, Appl. Catal. B: Environ. 88 (2009) 462–469.
[16] Y. Ding, L. Zhu, A. Huang, X. Zhao, X. Zhang, H. Tang, CatalSciTechnol 2 (2012) 1977–1984.
[17] Q. Yang, H. Choi, D.D. Dionysiou, Appl. Catal. B: Environ. 74 (2007) 170–178.
[18] Q. Yang, H. Choi, Y. Chen, D.D. Dionysiou, Appl. Catal. B: Environ. 77 (2008) 300–307.
[19] W. Zhang, H.L. Tay, S.S. Lim, Y. Wang, Z. Zhong, R. Xu, Appl. Catal. B: Environ. 95 (2010) 93–99.
[20] P. Shukla, H. Sun, S. Wang, H. Sun, H.M. Ang, M.O. Tadé, Sep. Purif. Technol. 77 (2011) 230–236.
[21] H. Liang, Y.Y. Ting, H. Sun, H.M. Ang, M.O. Tadé, S. Wang, J. Colloid Interface Sci. 372 (2012) 58–62.
[22] P. Shukla, S. Wang, H. Sun, H.M. Ang, M. Tadé, Appl. Catal. B: Environ. 100 (2010) 529–534.
[23] Y. Hardjono, H. Sun, H. Tian, C.E. Buckley, S. Wang, Chem. Eng. J. 174 (2011) 376–382.
[24] H. Sun, H. Tian, Y. Hardjono, C.E. Buckley, S. Wang, Catal. Today 186 (2012) 63–68.
[25] Y. Yao, Z. Yang, D. Zhang, W. Peng, H. Sun, S. Wang, Ind. Eng. Chem. Res. 51 (2012) 6044–6051.
[26] P. Shi, R. Su, F. Wan, M. Zhu, D. Li, S. Xu, Appl. Catal. B: Environ. 123–124 (2012) 265–272.
[27] P. Shi, R. Su, S. Zhu, M. Zhu, D. Li, S. Xu, J. Hazard. Mater. 229–230 (2012) 331–339.
[28] P. Shukla, S. Wang, K. Singh, H.M. Ang, M.O. Tadé, Appl. Catal. B: Environ. 99 (2010) 163–169.
[29] W. Chu, W.K. Choy, C.Y. Kwan, J. Agric. Food Chem. 55 (2007) 5708–5713.
[30] E. Grabowska, Appl. Catal. B: Environ. 186 (2016) 97–126.
[31] D.Q. Fei, T. Hudaya, A.A. Adesina, Catal. Commun. 6 (2005) 253–258.
[32] M. Misono, Catal. Today 144 (2009) 285–291.
[33] M. Misono, Studies in Surface Science and Catalysis, in: M. Makoto (Ed.), Elsevier, 2013, 2017, pp. 67–95.
[34] L.G. Tejuca, J.L.G. Fierro, J.M.D. Tascón, Advances in Catalysis, in: D.D. Eley, Herman Pines, B. Paul Weisz (Eds.), Academic Press, 1989, pp. 237–328 (2015).
[35] P. Kanhere, Z. Chen, Molecules 19 (2014) 19995–20022.
[36] W. Zhang, J. Tang, J. Ye, J. Mater. Res. 22 (2007) 1859–1871.
[37] S. Acharya, J. Mondal, S. Ghosh, S. Roy, P. Chakrabarti, Mater. Lett. 64 (2010) 415–418.
[38] J. Shi, L. Guo, Progr. Nat. Sci.: Mater. Int. 22 (2012) 592–615.
[39] H. Tanaka, M. Misono, Curr. Opin. Solid State Mater. Sci. 5 (2001) 381–387.
[40] J.L. Sotelo, G. Ovejero, F. Martínez, J.A. Melero, A. Milieni, Appl. Catal. B: Environ. 47 (2004) 281–294.
[41] J.E. Faye, J. Guélou, J. Barrault, J.M. Tatibouët, S. Valange, Top. Catal. 52 (2009) 1211–1219.
[42] O.P. Taran, A.B. Ayusheev, O.L. Ogorodnikova, I.P. Prosvirin, L.A. Isupova, V.N. Parmon, Appl. Catal. B: Environ. 180 (2016) 86–93.
[43] D. Sannino, V. Vaiano, P. Ciambelli, L.A. Isupova, Catal. Today 161 (2011) 255–259.
[44] R.R. Solís, F.J. Rivas, O. Gimeno, Appl. Catal. B: Environ. 200 (2017) 83–92.
[45] X. Pang, Y. Guo, Y. Zhang, B. Xu, F. Qi, Chem. Eng. J. 304 (2016) 897–907.
[46] M.R. Carrasco-Díaz, E. Castillejos-López, A. Cerpa-Naranjo, M.L. Rojas-Cervantes, Chem. Eng. J. 304 (2016) 408–418.
[47] J. Guo, Y. Dai, X. Chen, L. Zhou, T. Liu, J. Alloys Compd. 696 (2017) 226–233.
[48] V.A. Sadykov, L.A. Isupova, I.A. Zolotarskii, L.N. Bobrova, A.S. Noskov, V.N. Parmon, E.A. Brushtein, T.V. Telyatnikova, V.I. Chernyshev, V.V. Lunin, Appl. Catal. A: Gen. 204 (2000) 59–87.
[49] C. Su, X. Duan, J. Miao, Y. Zhong, W. Zhou, S. Wang, ACS Catal. 7 (2017) 388–397.
[50] J. Miao, J. Sunarso, C. Su, W. Zhaou, S. Wang, Z. Shao, Sci. Rep. 7 (2017) 44215, http://dx.doi.org/10.1038/srep44215.
[51] W. Xu, J. Cai, J. Zhou, Y. Ou, W. Long, Z. You, Y. Luo, ChemCatChem (2016) 417–425.
[52] M. Ao, G.-H. Pham, V. Sage, V. Pareek, J. Mol. Catal. A: Chem. 416 (2016) 96–104.
[53] Y. Zhu, R. Tan, J. Mater. Sci. 3 (5) (2000) 5415–5420.
[54] J.L. Hueso, A. Caballero, M. Ocaña, A.R. González-Elipe, J. Catal. 257 (2008) 334–344.
[55] L. Karvonen, S. Yoon, P. Hug, H. Yamauchi, A. Weidenkaff, M. Karppinenm, Mater. Res. Bull. 46 (2011) 1340–1345.
[56] A.S. Urusova, V.A. Cherepanov, T.V. Aksenova, L. Ya Gavrilova, E.A. Kiselev, J. Solid State Chem. 202 (2013) 207–214.
[57] H. Seim, M. Nieminen, L. Niinsto, H. Fjellvag, L.-S. Johansson, Appl. Surf. Sci. 112 (1997) 243–250.
[58] V. Stetsovych, F. Pagliuca, F. Dvořák, T. Duchoň, M. Vorokhta, M. Aulická, J. Lachnitt, S. Schernich, I. Matolínová, K. Veltruská, T. Skála, D. Mazur, J. Mysliveček, J. Libuda, V. Matolín, J. Phys. Chem. Lett. 4 (2013) 866–871.
[59] Y. Yang, Y. Jiang, Y. Wang, Y. Sun, J. Mol. Catal. A Chem. 270 (2007) 56–60.
[60] X. Zhao, Q. Yang, J. Cui, J. Rare Earth 26 (2008) 511–514.
[61] F. Ghanbari, M. Moradi, Chem. Eng. J. 310 (2017) 41–62.
[62] F. Qi, W. Chu, B. Xu, Appl. Catal. B 134–135 (2014) 324–332.
[63] J. Deng, Y. Shao, N. Gao, C. Tan, S. Zhou, X. Hu, J. Hazard. Mater. 262 (2013) 836–844.
[64] Y. Wang, X. Xie, S. Yin, R. XU, R. Lau, J. Taiwan Inst. Chem. Eng. 68 (2016) 246–253.
[65] Kun-Yi Andrew Lin, Yu-Chien Chen, J. Taiwan Inst. Chem. Eng. 60 (2016) 423–429.
[66] P. Shukla, H. Sun, S. Wang, H.M.A. Ng, M.O. Tade, Catal. Today 175 (2011) 380–385.
[67] E. Saputra, S. Muhammad, H. Sun, H.M. Ang, M.O. Tadé, S. Wang, Catal. Today 190 (2012) 68–72.
[68] X.Y. Chen, X.L. Qiao, D.G. Wang, J. Lin, J.W. Chen, Chemosphere 67 (2007) 802–808.
[69] L. Hu, X. Yang, S. Dang, Appl. Catal. B Environ. 102 (2011) 19–26.
[70] H. Liang, H. Sun, A. Patel, P. Shukla, Z.H. Zhu, S. Wang, Appl. Catal. B: Environ. 127 (2012) 330–335.
[71] W.D. OH, Z. Dong, T.T. Lim, Appl. Catal. B: Environ. 194 (2016) 169–201.
[72] D.G. Driscoll, J. Carter, J. Williamson, L. Putnam, Hydrology of the Black Hills 1441 Area, South Dakota, 2002.
[73] H. Gong, W. Chu, S.H. Lam, A.Y. Lin, Chemosphere 167 (2017) 415–421.
[74] Y.R. Wang, W. Chu, J. Hazard. Mater. 186 (2011) 1455–1461.
[75] X. Chen, J. Chen, X. Qiao, D. Wang, X. Cai, Appl. Catal. B: Environ. 80 (2008) 116–121.
[76] J. Li, Y. Yi, P. Shi, Q. Wang, D.X. Li, H. Asif, M. Yang, Acta Phys. – Chim. Sin. 30 (2014) 1720–1726.
[77] P. Hu, M. Long, Appl. Catal. B: Environ. 181 (2016) 103–117.
[78] H. Eibenberger, S. Steenken, P. O'Neill, D. Schulte-Frohlinde, J. Phys. Chem. 82 (1978) 749–750.
[79] B.S. Wolfenden, R.L. Willson, J. Chem. Soc. Perkin. Trans. II (1982) 805–812.
[80] K.-A. Lin, Y.C. Chen, C.-F. Huang, Sep. Purif. Technol. 170 (2016) 173–182.
[81] Y. Qian, X. Zhou, Y. Zhang, P. Sun, W. Zhang, J. Chen, X. Guo, X. Zhang, J. Chem. Eng. 279 (2015) 538–546.
[82] R. Chen, J.J. Pignatello, Environ. Sci. Technol. 31 (1997) 2399–2406.
[83] C. Petrier, M.-F. Lamy, A. Francony, A. Benahcene, B. David, V.N.G. Renaudin, Phys. Chem. A 98 (1994) 10514–10520.
[84] E. Mvula, C. Von Sonnntag, Org. Biomol. Chem. 1 (2003) 1749–1756.
[85] X. Li, J.W. Cubbage, T.A. Tetzlaff, W.S. Jenks, J. Org. Chem. 64 (1999) 8509–8524.
[86] J.A. Zazo, J.A. Casa, A.F. Mohedano, J.J. Rodriguez, Appl. Catal. B: Environ. 65 (2006) 261–268.